Supplementary Information for

Spin transition in magnesiowüstite and ultralow thermal conduction in ultralow velocity zones

Wen-Pin Hsieh[1,2]*, Frédéric Deschamps[1], Yi-Chi Tsao[1], Allison Pease[3], Susannah M. Dorfman[3], Hannah Bausch[4], and Fei Wang[5]

[1]Institute of Earth Sciences, Academia Sinica, Nankang, Taipei 11529, Taiwan
[2]Department of Geosciences, National Taiwan University, Taipei 10617, Taiwan
[3]Department of Earth and Environmental Sciences, Michigan State University, East Lansing, Michigan, USA
[4]Department of Earth, Environmental, and Planetary Sciences, Northwestern University, Illinois, USA
[5]Bayerisches Geoinstitut, University of Bayreuth, 95440 Bayreuth, Germany

Corresponding author: Wen-Pin Hsieh (wphsieh@earth.sinica.edu.tw)

Note S1. Synchrotron X-ray diffraction on the $(Mg_{0.25},Fe_{0.75})O$, Fp75, at high pressures

We performed synchrotron X-ray diffraction (XRD) measurements on the Fp75 at high pressures to ~89 GPa and room temperature at the beamline 12.2.2 of the Advanced Light Source, Lawrence Berkeley National Laboratory. We prepared two sets of samples within 200 μm culet diamond-anvil cells, loaded with silicone oil and neon as the pressure medium, respectively, and ruby and gold chips as pressure calibrants. Supplementary Fig. S1 shows the representative XRD patterns and spectra at selected pressures. When loaded with silicone oil as the medium (the same as our separate thermal conductivity measurements at room temperature), we found that the Fp75 remained a cubic structure at 16.8 GPa, while the (111) peak started to split at 23.5 GPa, suggesting a cubic to rhombohedral structural distortion. Fei *et al.*[1] observed a cubic to rhombohedral structural distortion in $(Mg_{0.42},Fe_{0.58})O$, Fp58, at ~44 GPa and made a phase diagram predicting the onset pressures for such distortion as a function of FeO content in (Mg,Fe)O. Our XRD observation is in good agreement with that suggested by Fei *et al.*[1], where the occurrence of structural distortion in Fp75 would be at ~20–30 GPa. Since we did not observe a significant change in the thermal conductivity of Fp75, Λ_{Fp75}, around this pressure range (Fig. 1 of the main text), the cubic to rhombohedral structural distortion seems to have minor effects on its thermal conductivity.

Supplementary Fig. S2 summarizes our present results for the pressure dependence of the unit-cell-volume of Fp75 along with relevant literature results with different FeO contents. Measurements with silicone oil (red circles) and with neon (red diamonds) as the medium consistently show an increase in compressibility at ~55 GPa, suggesting the onset of spin transition of iron. The different onset pressure and the pressure range for the spin transition in (Mg,Fe)O between the present and literature studies can be attributed to the different FeO content, characteristics of the sample (e.g., single-crystalline or polycrystalline powder), and the pressure medium used in each experiment, where nonhydrostatic stress induces the spin transition at lower pressures[1,2]. These XRD results suggest that the "sluggish" variation of the Λ_{Fp75} at P>~53 GPa in the Fig. 1 of the main text is presumably associated with the spin transition of iron. Though we did not perform high-pressure XRD on the Fp25, given its well-documented pressure range of spin transition[1,2], the decrease in Λ_{Fp25} between ~43 and 54 GPa (black symbols in the Fig. 1 of the main text) is expected to be resulted from the spin transition.

Note S2. Minor effect of the thermal pressure on the Λ_{Fp25} and Λ_{Fp75} at high temperature measurements

During the high temperature measurements, the pressure within the sample chamber inevitably is varied slightly due to the heating-induced thermal pressure. We, however, expect that such pressure variation does not significantly affect the temperature dependence we obtained (Fig. 3 of the main text). This is justified by the relatively weak pressure dependences of low-spin Λ_{Fp25} and Λ_{Fp75} within the pressure range of experiments, see their values in the low-spin state in Fig. 2 of the main text. For instance, the low-spin Λ_{Fp25} at 573 K and P=62–68 GPa (black symbols in Fig. 2 of the main text) minorly varies by <10%, which is less than the estimated data uncertainty. Therefore, the pressure variation (62–68 GPa) during the high temperature measurements (red symbols in Fig. 3a of the main text) can be treated as an essentially constant pressure. This treatment also applies to the low-spin Λ_{Fp75}, as the Λ_{Fp75} has an even weaker pressure dependence, see red symbols at P> ~60 GPa in Fig. 2 of the main text.

Note S3. Electrically insulating Fp25 and Fp75 at deep mantle conditions

The electrical conductivity σ of FeO wüstite and magnesiowüstite with FeO content higher than ~80% may increase as the *P-T* conditions approach those at the Earth's core-mantle boundary (CMB). For instance, the σ of $(Mg_{0.2},Fe_{0.8})O$, Fp80, at CMB's high *P-T* conditions was reported to increase to ~$10^{4.5}$ S m^{-1}, yet treated as an electrical insulator[3]. The σ of FeO at the CMB condition becomes ~10^{5} S m^{-1}, approaching that of an electrical conductor[4]. However, since the σ of (Mg,Fe)O is proportional to its FeO content[3,4], our samples (Fp75 and Fp25) with FeO content lesser than the Fp80 are expected to be more electrically insulating. In other words, the electrons have minor contributions to the Λ_{Fp25} and Λ_{Fp75} we presented in the Figs. 2 and 3 of the main text as well as the modelled profiles throughout the whole lower mantle in Fig. 4 of the main text.

Note S4. Mössbauer spectroscopy for ferric irons in Fp25 and Fp75 at room temperature

The Mössbauer spectra of our Fp samples display a dominant doublet and a weak shoulder on one side, which is very similar to those reported in the literature, e.g., Ref [5–7], and therefore were fitted to one doublet and one singlet. All fitting parameters are treated as free parameters. Although there is some variability, the fitted hyperfine parameters are in good agreement with the literature data[5–7]. The $Fe^{3+}/\Sigma Fe$ ratio were calculated from the relative areas, with the area of Fe^{3+} absorption constrained by the asymmetry of the main doublets, making it independent of the fitting model. The $Fe^{3+}/\sum Fe$ in Fp25 is ~6% and in Fp75 is ~12%, respectively (also see Supplementary Figure S5 and Table S2).

Mineral physics studies[8] have indicated that a simple Fe_2O_3 could undergo a series of phase transitions and reactions at deep mantle high *P*-*T* conditions, in which an oxygen-rich fluid could be present in the deep lower mantle and locally oxidize surrounding minerals. Since the (Mg,Fe)O is expected to be an important reservoir of ferric iron in the lower mantle[9], some amounts of ferric iron could be incorporated in Fe-rich magnesiowüstite at deep lower mantle.

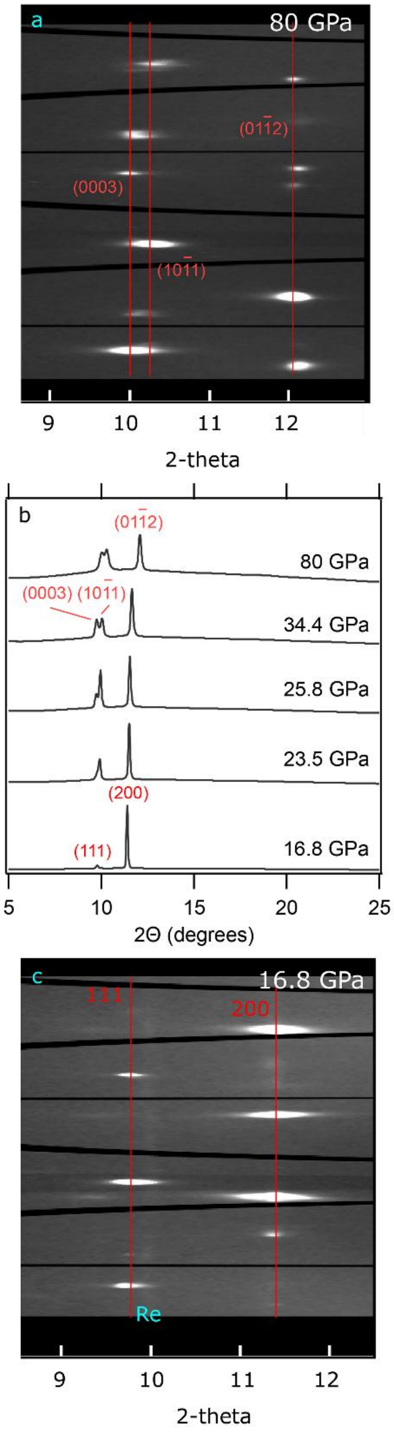

Supplementary Figure S1. Representative X-ray diffraction results for the Fp75 compressed in silicone oil. (a) Unrolled 2D diffraction image obtained at 80 GPa indicating diffraction spots for rhombohedral structure with labeled Miller indices. (b) Integrated diffraction intensity as a function of diffraction angle 2Θ for selected pressures. (c) Unrolled 2D diffraction image obtained at 16.8 GPa indicating diffraction spots for cubic B1 structure. Continuous background due to rhenium (Re) gasket is also observed at ~10°.

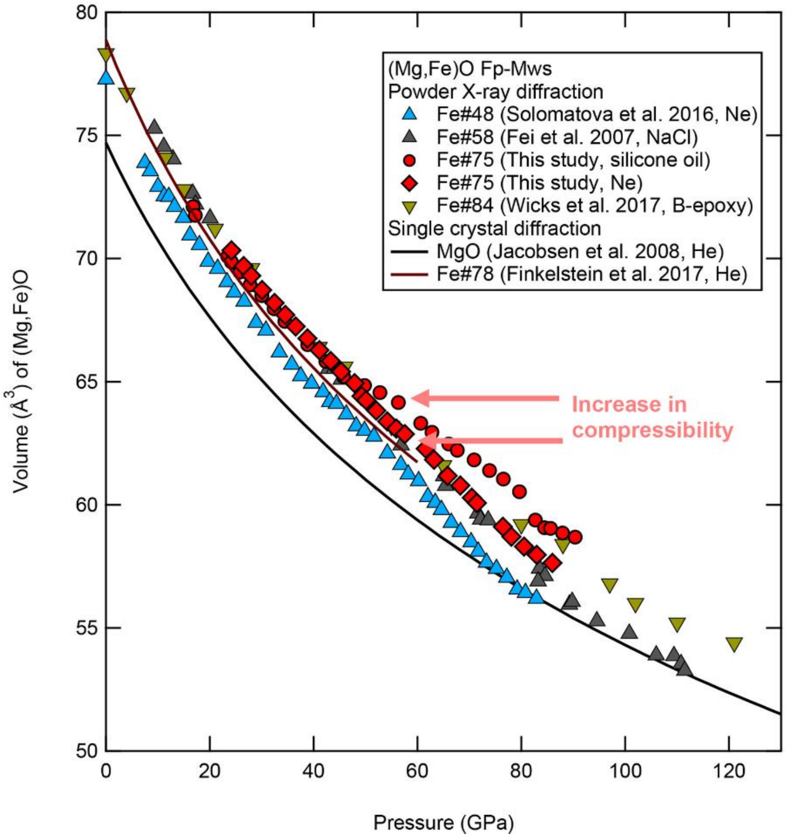

Supplementary Figure S2. Unit cell volume for Fp75 (this study, red symbols) as a function of pressure compressed in silicone oil and Ne media computed from (200) diffraction peak. Observations from previous studies of less iron-rich ferropericlase-magnesiowüstite[1,10] (up-pointing triangles) and more iron-rich compositions (down-pointing triangles) by powder[11] and single crystal[12,13] diffraction (curves) are also shown for comparison. Our two sets of Fp75 data consistently show an increase in compressibility at ~55 GPa, suggesting the onset of spin transition.

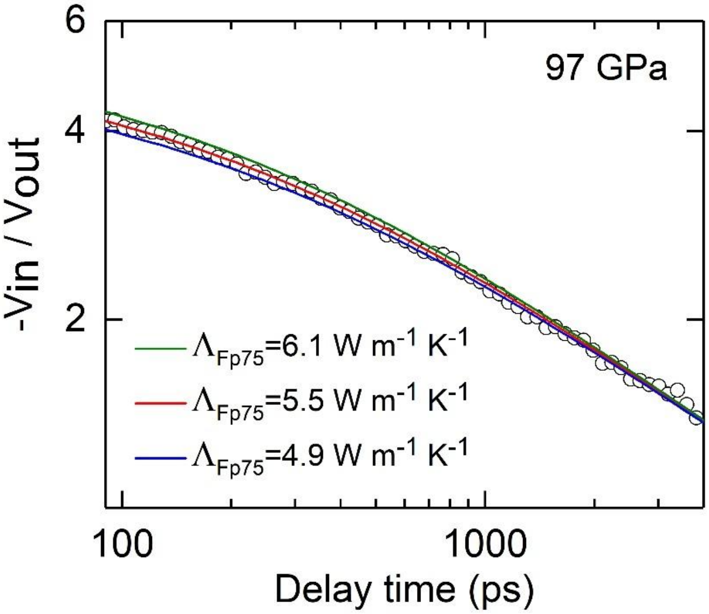

Supplementary Figure S3. Example TDTR data (open circles) for Fp75 at 97 GPa and room temperature along with thermal model calculations (color curves). The raw data are best-fitted with Λ_{Fp75}=5.5 W m^{-1} K^{-1} (red curve) using input model parameters listed in Supplementary Table S1. The data ratio of $-V_{in}/V_{out}$ is most sensitive to the thermal conductivity of Fp75 at few hundred picosecond (ps) delay time[14,15]. Minor changes by ±10% in the Λ_{Fp75} lead to clear mis-fits to the data, which indicate the high sensitivity of the thermal model fitting to our high-quality data with precise Λ_{Fep75}.

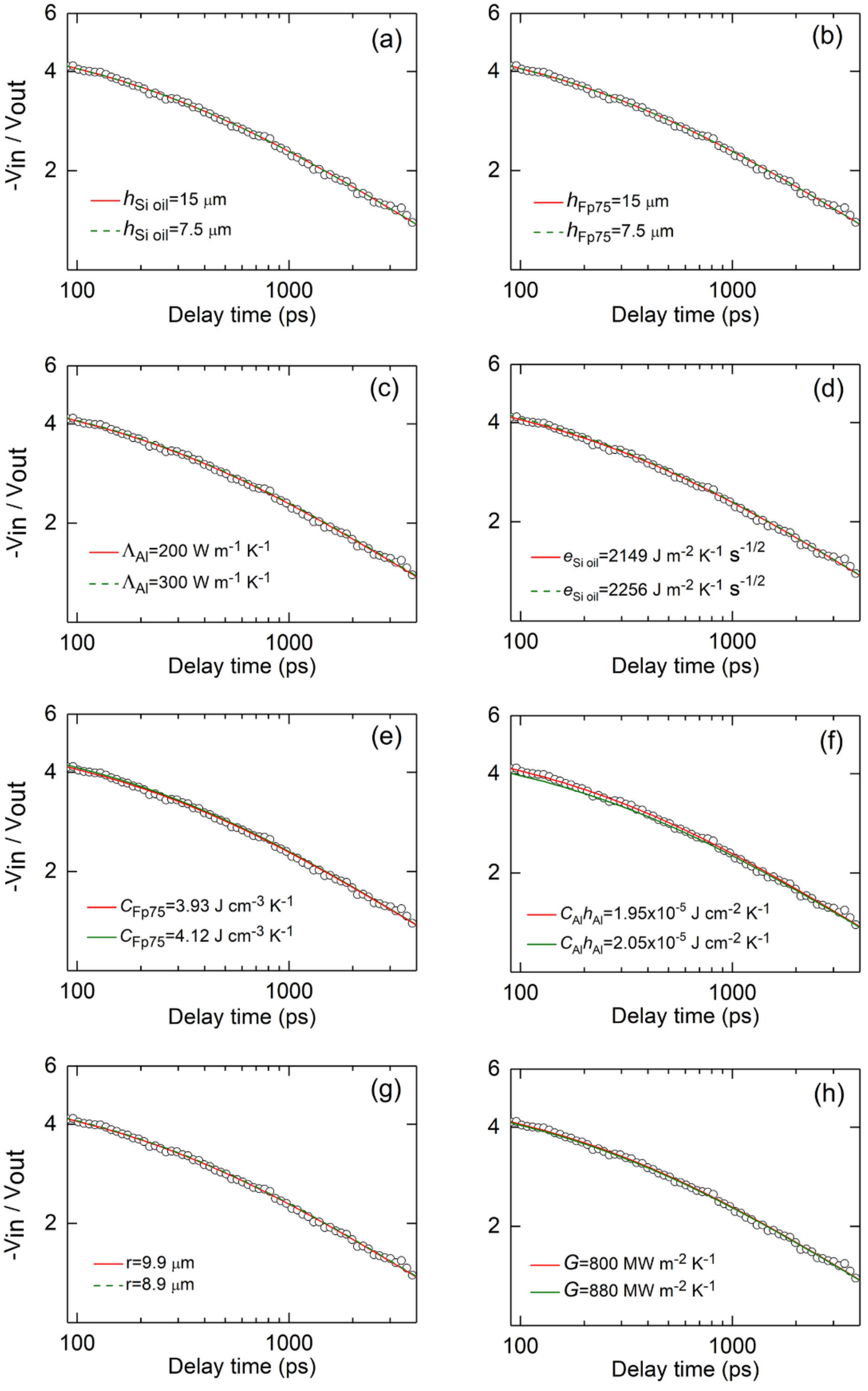

Supplementary Figure S4. Standard sensitivity tests of the thermal model calculations to key parameters for Fp75 at 97 GPa and room temperature. Here the Fp75's thermal conductivity, Λ_{Fp75}, is fixed at 5.5 W m^{-1} K^{-1} as derived from Supplementary Fig. S3. **(a)** and **(b)** Even though the thickness of silicone oil ($h_{\mathrm{Si\ oil}}$) and Fp75 sample (h_{Fp75}), respectively, changes by 50%, the thermal model calculation remains the same, verifying that their uncertainty does not affect the derived Λ_{Fp75}. (**c)** Since the Al's thermal conductivity is fairly high at high pressures, an uncertainty as large as 50% does not influence the Λ_{Fp75}. (**d)** If the thermal effusivity of the silicone oil pressure medium, $e=(\Lambda_{\mathrm{Si}}C_{\mathrm{Si}})^{1/2}$, is off by 5%, the data can be re-fitted with a smaller Λ_{Fp75} of 5.4 W m^{-1} K^{-1}, i.e., translating ~1.8% error for the derived Λ_{Fp75}. (**e)** If the volumetric heat capacity of Fp75, C_{Fp75}, is off by 5%, the data can be re-fitted also with a smaller Λ_{Fp75} of 5.4 W m^{-1} K^{-1}, again, minorly translating ~1.8% error. (**f)** The uncertainty in the heat capacity of Al per unit area (product of Al's volumetric heat capacity and thickness, $C_{\mathrm{Al}}\,h_{\mathrm{Al}}$)[14] is the major source of error for our data analysis. If it is off by 5%, for example, the data can be re-fitted with a larger Λ_{Fp75} of 6.1 W m^{-1} K^{-1} (i.e., ~10% error). Finally, an example 10% error for the (**g)** laser spot size and (**h**) thermal conductance of Al/silicone oil and Al/Fp75 interfaces, G, respectively, does not influence the thermal model calculations, indicating that these uncertainties have essentially no effect on the Λ_{Fp75}.

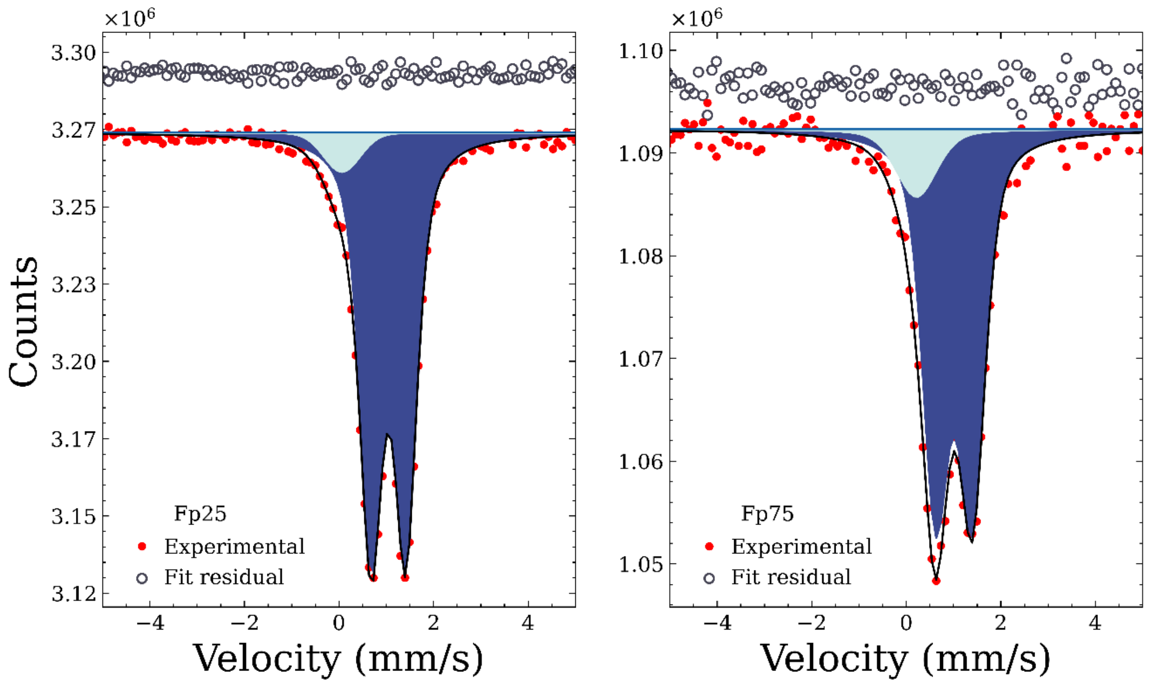

Supplementary Figure S5. Mössbauer spectra of Fp samples. The doublets are Fe^{2+} in Fp in dark blue, while Fe^{3+} in Fp is in cyan.

Supplementary Table S1. Input parameters in the thermal model for Fp75 at 97 GPa and room temperature in TDTR measurements

P (GPa)	C_{Fp75} (J cm^{-3} K^{-1})	C_{Al} (J cm^{-3} K^{-1})	h_{Al} (nm)*	$e=(\Lambda_{\mathrm{Si}}C_{\mathrm{Si}})^{1/2}$ (J m^{-2} K^{-1} s$^{-1/2}$)	r (μm)	$h_{\mathrm{Si\ oil/Fp75}}$ (μm)	Λ_{Al} (W m^{-1} K^{-1})	G (MW m^{-2} K^{-1})
97	3.93	2.684	72.6	2149	9.9	15/15	200	800

*In this experimental run, the Al's thickness at ambient pressure is 87.3 nm.

C_{Fp75}: Fp75's heat capacity, C_{Al}: Al's heat capacity, h_{Al}: Al's thickness, e: silicone oil's thermal effusivity, r: laser spot size, $h_{\mathrm{Si\ oil}}$: silicone oil's thickness, h_{Fp75}: Fp75's thickness, Λ_{Al}: Al's thermal conductivity, G: thermal conductance of Al/Fp75 and Al/silicone oil interfaces.

Supplementary Table S2. Best fit hyperfine parameters of the Mössbauer spectra and the Fe^{3+}/∑Fe ratios in Fp25 and Fp75.

	Fe^{2+}			Fe^{3+}			
	CS (mm/s)	QS (mm/s)	Area	CS (mm/s)	QS (mm/s)	Area	Fe^{3+}/ΣFe
Fp25	1.046(6)	0.729(8)	94(3)	0.06(9)	Not applicable	6(3)	6(3) %
Fp75	1.01(2)	0.77(3)	88(7)	0.2(1)	Not applicable	12(7)	12(7) %

Supplementary References

1. Fei, Y. *et al.* Spin transition and equations of state of (Mg,Fe)O solid solutions. *Geophys Res Lett* **34**, L17307 (2007).
2. Lin, J.-F., Speziale, S., Mao, Z. & Marquardt, H. Effects of the Electronic Spin Transitions of Iron in Lower Mantle Minerals: Implications for Deep Mantle Geophysics and Geochemistry. *Reviews of Geophysics* **51**, 244–275 (2013).
3. Ohta, K. *et al.* Highly conductive iron-rich (Mg,Fe)O magnesiowüstite and its stability in the Earth's lower mantle. *J Geophys Res Solid Earth* **119**, 4656–4665 (2014).
4. Ho, W. G. D. *et al.* Quantum critical phase of FeO spans conditions of Earth's lower mantle. *Nat Commun* **15**, 3461 (2024).
5. McCammon, C. A., Stachel, T. & Harris, J. W. Iron oxidation state in lower mantle mineral assemblages II. Inclusions in diamonds from Kankan, Guinea. *Earth Planet Sci Lett* **222**, 423–434 (2004).
6. Dobson, D. P., Cohen, N. S., Pankhurst, Q. A. & Brodholt, J. P. A convenient method for measuring ferric iron in magnesiowüstite (MgO-Fe1-xO). *American Mineralogist* **83**, 794–798 (1998).
7. Otsuka, K., Longo, M., McCammon, C. A. & Karato, S. ichiro. Ferric iron content of ferropericlase as a function of composition, oxygen fugacity, temperature and pressure: Implications for redox conditions during diamond formation in the lower mantle. *Earth Planet Sci Lett* **365**, 7–16 (2013).
8. Bykova, E. *et al.* Structural complexity of simple Fe2O3 at high pressures and temperatures. *Nat Commun* **7**, 10661 (2016).
9. Stixrude, L. & Lithgow-Bertelloni, C. Thermodynamics of mantle minerals – III: the role of iron. *Geophys J Int* **237**, 1699–1733 (2024).
10. Solomatova, N. V. *et al.* Equation of state and spin crossover of (Mg,Fe)O at high pressure, with implications for explaining topographic relief at the core-mantle boundary. *American Mineralogist* **101**, 1084–1093 (2016).
11. Wicks, J. K., Jackson, J. M., Sturhahn, W. & Zhang, D. Sound velocity and density of magnesiowüstites: Implications for ultralow-velocity zone topography. *Geophys Res Lett* **44**, 2148–2158 (2017).

12. Finkelstein, G. J. *et al.* Single-crystal equations of state of magnesiowüstite at high pressures. *American Mineralogist* **102**, 1709–1717 (2017).
13. Jacobsen, S. D. *et al.* Compression of single-crystal magnesium oxide to 118 GPa and a ruby pressure gauge for helium pressure media. *American Mineralogist* **93**, 1823–1828 (2008).
14. Zheng, X., Cahill, D. G., Krasnochtchekov, P., Averback, R. S. & Zhao, J. C. High-throughput thermal conductivity measurements of nickel solid solutions and the applicability of the Wiedemann-Franz law. *Acta Mater* **55**, 5177–5185 (2007).
15. Cahill, D. G. & Watanabe, F. Thermal conductivity of isotopically pure and Ge-doped Si epitaxial layers from 300 to 550 K. *Phys. Rev. B* **70**, 235322 (2004).